First posted online on 28 September 2018 as 10.1242/dmm.035311
Access the most recent version at http://dmm.biologists.org/lookup/doi/10.1242/dmm.035311

Overexpression of *Fgfr2c* causes craniofacial bone hypoplasia and ameliorates craniosynostosis in the Crouzon mouse

Kevin KL Lee[1], Emma Peskett[1, 2], Charlotte M Quinn[1], Rosanna Aiello[1], Liliya Adeeva[1], Dale A Moulding[3], Philip Stanier[2], Erwin Pauws[1]

[1]Developmental Biology & Cancer Programme; [2]Genetics & Genomic Medicine Programme; [3]ICH GOSH Light Microscopy Core Facility. UCL Great Ormond Street Institute of Child Health, 30 Guilford Street, London WC1N 1EH, United Kingdom

Key words

FGFR2, FGF, craniosynostosis, cleft palate, Crouzon, ERK

Highlights

- *Fgfr2c* overexpression causes craniofacial hypoplasia, microtia and cleft palate.
- Craniosynostosis is not associated with *Fgfr2c* overexpression.
- Mutant coronal sutures have increased levels of MAPK/ERK signalling.
- *Fgfr2c* overexpression partially rescues craniosynostosis in the Crouzon mouse.

Summary statement

Increased levels of FGFR2c cause craniofacial bone hypoplasia, microtia and cleft palate, but not craniosynostosis. Introduction of an extra *Fgfr2c* allele into a mouse model for Crouzon syndrome partially rescues the craniosynostosis phenotype.

Abstract

FGFR2c regulates many aspects of craniofacial and skeletal development. Mutations in the FGFR2 gene are causative for multiple forms of syndromic craniosynostosis, including Crouzon syndrome. Paradoxically, mouse studies have shown that both the activation (*Fgfr2c*^{C342Y}; a mouse model for human Crouzon syndrome), as well as the removal (*Fgfr2c*^{null}) of the FGFR2c isoform can drive suture abolishment. This study aims to address the downstream effects of pathogenic FGFR2c signalling by studying the effects of *Fgfr2c* overexpression.

Conditional overexpression of *Fgfr2c* (*R26R*$^{Fgfr2c;\beta act}$) results in craniofacial hypoplasia as well as microtia and cleft palate. Contrary to *Fgfr2c*^{null} and *Fgfr2c*^{C342Y}, *Fgfr2c* overexpression is insufficient to drive onset of craniosynostosis. Examination of the MAPK/ERK pathway in the embryonic sutures of *Fgfr2c*^{C342Y} and *R26R*$^{Fgfr2c;\beta act}$ mice reveals that both mutants have increased pERK expression. The contrasting phenotypes between *Fgfr2c*^{C342Y} and *R26R*$^{Fgfr2c;\beta act}$ mice prompted us to assess the impact of the *Fgfr2c* overexpression allele on the Crouzon mouse (*Fgfr2c*^{C342Y}), in particular to the coronal suture. Our results demonstrate that *Fgfr2c* overexpression is sufficient to partially rescue craniosynostosis through increased proliferation and reduced osteogenic activity in E18.5 *Fgfr2c*^{C342Y} embryos.

This study demonstrates the intricate balance of FGF signalling required for correct calvarial bone and suture morphogenesis, and that increasing the expression of the wild-type FGFR2c isoform may be a way to prevent or delay craniosynostosis progression.

Introduction

Normal craniofacial development is a precisely coordinated process that involves the modelling of a framework supporting the soft tissues of the head, in particular the brain. During normal development, growth of the brain is possible because suture tissue separates the calvarial bones and allows for skull vault expansion. Craniosynostosis, a common birth defect with an incidence of 1:2,500, is characterised by the loss of suture tissue followed by premature fusion of calvarial bones. This results in the restriction of brain growth and is often associated with dramatic dysmorphology of the skull and face. A significant number of craniosynostosis cases are syndromic and associated with additional skeletal phenotypic features. Many of these syndromes are caused by mutations in FGF pathway genes (Johnson and Wilkie, 2011).

FGF signalling is important for cellular proliferation, differentiation and survival. Receptor activation allows signals to be conveyed through the RAS-MAPK, P13K-AKT and PLCγ-PKC cascades via a series of protein intermediates (Ornitz and Itoh, 2015, Eswarakumar et al., 2005). FGF receptors (FGFRs) are highly conserved receptor tyrosine kinases (RTKs) located on the cell membrane with intracellular and extracellular domains. Tissue specific isoforms are produced by alternative splicing, affecting the third extracellular immunoglobulin-like loop (DIII) of FGFR1-3. The FGFR 'IIIb' and 'IIIc' isoforms differ only in the C-terminal half of DIII, which is encoded by exons 8 or 9 for the IIIb and IIIc splice forms respectively (Eswarakumar et al., 2005, Ornitz and Itoh, 2015). Furthermore, the expression of the isoforms are tissue specific and critical for establishing paracrine reciprocal signalling loops: while the IIIb isoform is commonly expressed in epithelial cells and receives FGF ligand from the mesenchyme, the IIIc is expressed in mesenchymal cells and receives FGF ligand from the neighbouring epithelium (Orr-Urtreger et al., 1993).

Mutations affecting the *FGFR2* gene can cause a spectrum of craniofacial phenotypes commonly associated with growth dysplasia, mid-facial hypoplasia, coronal synostosis, orbit dysmorphology and cleft palate (Wilkie, 1997). Notably, synostosis of the coronal suture is a hallmark for human Crouzon-Pfeiffer syndromes (CPS) (Johnson and Wilkie, 2011). Crouzon syndrome is most commonly caused by a point mutation in exon 9 of the *FGFR2* gene, is autosomal dominantly

inherited and exclusively affects the IIIc isoform (Reardon et al., 1994). The substitution of a cysteine to a tyrosine residue (p.C342Y) results in the stabilization of intermolecular disulphide bonds in the receptor extracellular domains that lead towards ligand independent receptor activation and is often referred to as a gain-of-function (GOF) mutation (Reardon et al., 1994).

In the developing mouse cranial vault, *Fgfr2* is expressed in the osteogenic fronts of the calvarial bones, but the specific cellular localisation of the different *Fgfr2* isoforms remains elusive due to their high sequence homology (Johnson et al., 2000, Iseki et al., 1997). FGFR2c function is commonly associated with craniofacial and skeletal development as genetic mutation in mouse models leads to a series of craniofacial malformations and additional skeletal dysmorphology (Lee et al.). Deletion of the FGFR2c isoform (*Fgfr2c*^{null}) results in skeletal hypoplasia and craniosynostosis due to imbalances in osteoprogenitor proliferation and differentiation in the endochondral as well as the intramembranous skeleton (Eswarakumar et al., 2002). The most common coding mutation responsible for human Crouzon syndrome has been introduced into the mouse (*Fgfr2c*^{C342Y}) to study the pathogenesis of the disease in more detail (Eswarakumar et al., 2004). The craniofacial phenotype in these mice includes brachycephaly due to postnatal coronal craniosynostosis, as well as a short snout caused by midfacial hypoplasia (Eswarakumar et al., 2004). Contrary to *Fgfr2c*^{null} mice, increased numbers of osteoprogenitor cells were observed, but paradoxically, synostosis of the coronal suture was also present (Eswarakumar et al., 2004). Recently, it was shown that increased levels of MAPK/ERK signalling downstream of FGFR2c are present in suture osteoprogenitors in *Fgfr2c*^{C342Y} but not *Fgfr2c*^{null} mice (Pfaff et al., 2016). In addition, hemizygous mutants (*Fgfr2c*$^{C342Y/-}$) show a more severe craniofacial phenotype, demonstrating that lowering the *Fgfr2c* expression levels does not alleviate the features associated with FGFR2c activation (Pfaff et al., 2016). Altogether, the mechanism behind pathogenic FGFR2c signalling in the coronal suture is complex as indicated by the observation that coronal synostosis is a notable phenotype to both activation (*Fgfr2c*^{C342Y}) and loss (*Fgfr2c*^{null}) of FGFR2 signalling (Eswarakumar et al., 2002, Eswarakumar et al., 2004). Furthermore, analysis of the cleft palate phenotype in *Fgfr2c*^{C342Y} mice demonstrates that activation as well as inhibition of FGF receptor signalling causes delayed palatal shelf growth and elevation (Snyder-

Warwick et al., 2010). These results imply that the downstream interpretation of FGFR2c signalling can be different to the activity of the receptor itself, and the phenotype elicited may not be a direct translation of an overactive FGFR2c signalling pathway.

The complexities of FGFR2c signalling prompted us to delineate the molecular basis for signalling misregulation further by studying *Fgfr2c* receptor overexpression using a conditional allele that allows tissue-specific induction (i.e. $R26R^{Fgfr2c\text{-}flox}$). This study reports that the phenotypic consequences of *Fgfr2c* overexpression show similarities as well as differences to those found in $Fgfr2c^{C342Y}$ and $Fgfr2c^{null}$ mice. We have interrogated the biochemical and transcriptional FGFR2 pathway activity in the coronal sutures prior to the onset of synostosis, and show that both constitutive activation and overexpression of FGFR2c results in increased levels of ERK phosphorylation *in vivo*. Furthermore, we provide evidence that increasing the expression of a wild-type *Fgfr2c* allele can ameliorate the craniosynostosis phenotype in $Fgfr2c^{C342Y}$ Crouzon mice.

Results

Fgfr2c overexpression causes growth restriction, microtia and cleft palate.

To assess which tissues are sensitive to increased FGFR2c signalling, *R26R*$^{Fgfr2c\text{-}flox}$ mice were crossed with *βactin*^{CRE} mice to drive ubiquitous *Fgfr2c* overexpression (**Figure 1A**). Ubiquitous overexpression of the *R26R*^{Fgfr2c} allele (i.e. *R26R*$^{Fgfr2c\text{-}flox}$; *βactin*^{CRE} abbreviated to *R26R*$^{Fgfr2c;\beta act}$) led to a total upregulation of *Fgfr2c* transcripts close to 2-fold (n=3) as shown by qPCR (**Supplementary Figure 1A**) at E12.5. Transgenic FGFR2c-V5 protein expression was validated at E12.5 by immunoblotting showing transgenic protein in the CRE positive animals only (**Supplementary Figure 1B**). Subsequently, *R26R*$^{Fgfr2c;\beta act}$ embryos were examined at E18.5 for their size (Head Length and Crown Rump Length (CRL)) and weight (**Figure 1C, D** and **E**). Results were expressed as an average percentage change (Av.Δ %) relative to controls (*R26R*$^{Fgfr2c\text{-}flox}$). Ubiquitous *Fgfr2c* overexpression (n=9) led to a significant reduction in the head length (Av.Δ 7.19%; $p<0.0001$; $t(17.78)=7.74$), CRL (Av.Δ 4.83%; $p=0.0018$; $t(13.23)=3.90$) and weight (Av.Δ 12.26%; $p=0.0001$; $t(22.16)=5.39$) to controls (*R26R*$^{Fgfr2c\text{-}flox}$; n=17) (**Figure 1C**, **D** and **E**). Additionally, *R26R*$^{Fgfr2c;\beta act}$ mice display microtia characterised by a smaller or absent pinna (n=6/6) (**Figure 1B**). To assess whether decreased size was due to generalised defects of the whole skeleton we analysed limb length as a proxy for this (**Supplementary Figure 2**). No difference in the size of the limbs (n=13) was detected, suggesting that the overall size reduction was mostly due to reduced head size. Whole mount skeletal staining of the head showed that mutants had craniofacial dysmorphology showing notable disruptions to the tympanic ring of the middle ear (n=9/10) and a cleft palate (n=4/10) (**Figure 2A**). As different parts of the calvaria are derived from either the neural crest or mesodermal lineage (Yoshida et al., 2008), *R26R*$^{Fgfr2c\text{-}flox}$ animals were subsequently crossed with *Wnt1*^{CRE} or *Mesp1*^{CRE} to ask which cell types are responsible for the observed phenotypes, and to eliminate any potential ectopic effects generated by the ubiquitous *βactin*^{CRE} line. To assess the promoter activity of the different CRE lines specifically in calvarial tissues we investigated conditional fluorescent alleles (i.e. mTmG and YFP). We found that expression was robust and specific for all CRE lines (**Supplementary Figure 3**). *R26R*$^{Fgfr2c;Wnt1}$ embryos (n=6) showed a significant decrease in weight

(Δ12.26%; p=0.0028; t(9.23)=4.05) while head length and CRL were not significantly reduced (**Figure 1C**, **D** and **E**). Moreover, the clefting phenotype was heterogeneous in its severity: 1 out of 6 embryos exhibit an overt cleft whilst 3 out of 6 display palatal shelf hypoplasia (data not shown) (**Figure 2A**). In contrast to *R26R*$^{Fgfr2c;\beta act}$ mice, middle (tympanic ring) or outer (pinna) ear defects were absent in this cohort of embryos (n=0/6) (**Figure 2A**). In *R26R*$^{Fgfr2c;Mesp1}$, no defects were present in the ear or the palate (n=0/9) (**Figure 2A**) and no significant effects on size were seen in embryos upon *Fgfr2c* overexpression in the mesoderm using *Mesp1*^{CRE} (n=9) compared to controls (n=4) (**Figure 1C**, **D** and **E**). Together, ubiquitous and conditional *Fgfr2c* overexpression in the neural crest lineage stunts overall growth resembling the phenotypic effect of *Fgfr2c*^{null} knockout mice. Additionally, *Fgfr2c* overexpression mutants display microtia and cleft palate, of which the latter is also found in *Fgfr2c*^{C342Y} mutants, but has not been identified in *Fgfr2c*^{null} mice.

***Fgfr2c* overexpression causes anterior, neural crest derived bone hypoplasia.**

As all observed phenotypic features in *R26R*^{Fgfr2c} mice seem to affect tissues in the head, we assessed the craniofacial morphology in more detail at E18.5 using Alcian Blue/Alizarin Red whole-mount skeletal staining and quantified the size and shape of individual craniofacial bones. The results were expressed as an average percentage change in the mutants relative to the controls (*R26R*$^{Fgfr2c\text{-}floxed}$) normalised to 100% (Av.Δ %). Frontal bones of *R26R*$^{Fgfr2c;\beta act}$ skulls were significantly smaller (Av.Δ11.4%; p<.0001; t(22.98)=6.99; n=9) (**Figure 2B** and **C**) along with other neural crest derivatives such as nasal bone (Av.Δ 12.90%; p<0.0001; t(22.06)=7.91; n=10) and mandible (Av.Δ 5.77%; p<0.0001; t(20.64)=7.30; n=9) (**Supplementary Figure 4**). No significant reduction was observed in the mesoderm-derived parietal bone. Similarly, *R26R*$^{Fgfr2c;Wnt1}$ embryos followed a comparable trend with significant decreases in neural crest derivatives: frontal bone (Av Δ9.12%; p=.0131; t(6.89)=3.32; n=6), nasal bone (Av.Δ 7.91%; p=.0024; t(9.077)=4.17; n=6); and mandible (Av.Δ3.71%) (p=.0007; t(9.96)=4.82; n=6). Again, no size difference was seen in the mesoderm-derived parietal bone (n=6). As expected, in *R26R*$^{Fgfr2c;Mesp1}$ mice, calvarial bone sizes were not affected. In summary, *Fgfr2c* overexpression causes bone hypoplasia of anterior, neural crest derived bones, explaining the overall reduction of craniofacial dimensions.

Fgfr2c overexpression does not cause coronal craniosynostosis.

Coronal synostosis is a hallmark of Crouzon-Pfeiffer syndrome and can be observed in the *Fgfr2c*^{C342Y} mouse model as well as the *Fgfr2c*^{null} mice. While subtle changes in the *Fgfr2c*^{C342Y} heterozygous coronal suture morphology are visible from E17.5, full fusion of frontal and parietal bones is not visible until three weeks after birth. Due to the presence of a cleft palate in *R26R*$^{Fgfr2c;\beta act}$ embryos, mice do not survive after birth, making it impossible to assess the postnatal synostosis phenotype. *Ex vivo* explant cultures were adopted to overcome this problem. Calvarial explant cultures in our laboratory routinely show that coronal synostosis can be achieved *in vitro* after 1-2 weeks of culture in *Fgfr2c*^{C342Y} heterozygote E17.5 explants. In *R26R*$^{Fgfr2c;\beta act}$ calvaria, coronal synostosis was not observed (n=6), similar to wild-type and *R26R*$^{Fgfr2c\text{-}floxed}$ controls (n=7). At the same time, *Fgfr2c*^{C342Y} heterozygous coronal sutures are reduced in size and signs of suture fusion can be observed after 15 days in culture (**Figure 3**). Additionally, we have examined the effect of FGFR2 perturbation on osteoblast maturation at a pre-synostosis embryonic stage (E16.5) by analysing alkaline phosphatase (ALP) activity. In all cases, *Fgfr2c*^{C342Y} heterozygous sutures display increased suture overlap and ectopic ALP in the sutural mesenchyme (n=3) whilst *R26R*$^{Fgfr2c;\beta act}$ frontal and parietal bones are spaced normally and resemble controls (n=3) (**Figure 4**). This data implies that FGFR2c overexpression does not cause coronal craniosynostosis and does not mimic FGFR2 activation in the *Fgfr2c*^{C342Y} suture.

FGFR2c overexpression and FGFR2c-C342Y mutation activate MAPK/ERK signalling in the suture.

To assess whether *Fgfr2c* overexpression leads to a similar activation of the MAPK/ERK pathway as found in the *Fgfr2c*^{C342Y} mouse, we looked at levels of pERK in the suture *in vivo* and *in vitro*. We sought to visualise the expression of pERK in E16.5 coronal sutures using immunohistochemistry at a stage where the sutures were morphologically similar, i.e. prior to the onset of synostosis (*R26R*$^{Fgfr2c;\beta act}$, n=3; *Fgfr2c*$^{C342Y/+}$, n=4; control, n=4). Interestingly, both *Fgfr2c*$^{C342Y/+}$ and *R26R*$^{Fgfr2c;\beta act}$ mutants showed upregulated pERK in the osteogenic fronts of frontal and parietal bones

flanking the suture (**Figure 5A**). We have also modelled pERK activity *in vitro* using the human embryonic kidney (HEK293T) cell line (n=4 independent transfections). pERK 1 and 2 were activated upon transfection of pFGFR2c(WT)V5 (encoding the wild-type FGFR2-IIIc isoform) and pFGFR2c(C342Y)V5 (encoding the mutated receptor) relative to mock transfected cells (**Figure 5B**). Quantification of the blots using densitometry reveals significant upregulation of pERK in both FGFR2cV5 transfected conditions (**Figure 5C**). Specifically, there was significantly more pERK activity in the C342Y-V5 ($p<0.0001$) and WT-V5 ($p=0.0101$) transfected cells relative to the pcDNA3.1 control cells as expected from the Western blot results. Cells transfected with C342Y-V5 has an increased pERK output by 8.1 units than that of WT-V5 transfected group ($p=0.0005$) likely due to the constitutive activation of the mutant receptor. While both models show an activated RAS-MAPK pathway in the suture, the fact that only *Fgfr2c*^{C342Y} activation results in craniosynostosis suggest that FGFR2c overexpression cascade activation is functionally distinct to that of the mutant receptor.

Introduction of the *Fgfr2c* overexpression allele into *Fgfr2c*^{C342Y} mice delays craniosynostosis.

As FGFR2c overexpression does not cause coronal suture synostosis, we hypothesized whether the addition of this allele to the *Fgfr2c*^{C342Y} mice would modify the craniofacial phenotype. To assess the impact of the overexpression allele, we have generated a double mutant (i.e. *R26R*$^{Fgfr2c;\beta act}$;*Fgfr2c*^{C342Y}) and performed quantitative analysis on the calvaria as before (**Figure 6**). The most apparent external anomaly resulting from *Fgfr2c* overexpression alone was microtia. This was exacerbated in double mutants where anotia was present in 90% of mice (**Figure 6A**) (n=10/11). External ear development was normal in all *Fgfr2c*^{C324Y} single mutants (n=15). Double mutants showed cleft palate with an increased penetrance (n=7/7). Examination of the craniofacial skeleton reveals partial rescue of the Crouzon phenotype: an ectopic interfrontal Wormian bone is characteristic of *Fgfr2c*^{C342Y} heterozygotes (n=6/7), and these were generally smaller in double mutants (n=4/5) combined with an enlarged widening of the posterior interfrontal suture (**Figure 6B**). In general, quantitative analyses of calvarial bones show that *R26R*$^{Fgfr2c;\beta act}$;*Fgfr2c*^{C342Y} frontal bones were smaller than those of controls (Av.Δ11.86; $p<0.001$; control: n=8, double mutant: n=6) (**Figure**

6C). Significance size reduction was present when *R26R*$^{Fgfr2c;\beta act}$ frontal bones (n=6) were compared to *Fgfr2c*^{C342Y} (n=10)(Av.Δ 9.19%; p=0.001). Also, there was a significant decrease in frontal bone size between *R26R*$^{Fgfr2c;\beta act}$;*Fgfr2c*^{C342Y} and *Fgfr2c*^{C342Y} (Av.Δ 14.80%; p<0.001). Quantitative analysis of the parietal bones indicates significant increase in the parietal bone of *Fgfr2c*^{C342Y} (n=10) as compared to all other genotypes (control: Av.Δ6.54%, p=0.001, n=8; *R26R*$^{Fgfr2c;\beta act}$ Av.Δ6.08%, p=0.006, n=6; *R26R*$^{Fgfr2c;\beta act}$;*Fgfr2c*^{C342Y}: Av.Δ5.44%, p=0.016, n=6) (**Figure 6D**). Most strikingly, coronal sutures in double mutants appeared more patent than those in *Fgfr2c*^{C342Y} alone. Frontal and parietal bone overlap was decreased in *R26R*$^{Fgfr2c;\beta act}$;*Fgfr2c*^{C342Y} coronal sutures shown by Alizarin Red stain and ALP activity (**Figure 6B**) (control: n=2; *Fgfr2c*$^{C342Y:}$ n=2; *R26R*$^{Fgfr2c;\beta act}$;*Fgfr2c*^{C342Y}: n=3). However, the observed ectopic ALP in the sutural mesenchyme of *Fgfr2c*^{C342Y} animals (see **Figure 4**) was not decreased in the majority of double mutant sutures (**Figure 6B**). This suggests that the overexpression allele is potentially only delaying the synostosis process, possibly through calvarial bone hypoplasia caused by decreased osteogenic differentiation or increased mesenchymal proliferation.

Increased proliferation in *R26R*$^{Fgfr2c;\beta act}$;*Fgfr2c*^{C342Y} double mutants.

To test the hypothesis that altered proliferation in the suture underlies the delayed onset of craniosynstosis in *R26R*$^{Fgfr2c;\beta act}$;*Fgfr2c*^{C342Y} double mutants, we performed phoshohistone-3 (PHH3) immunohistochemistry to assess mitotic index (**Figure 7A**). While levels of proliferation were unchanged in the periosteum overlying the coronal suture, a statistically significant (P<0.05) increase was detected in the sutural mesenchyme of double mutants compared to *Fgfr2c*^{C342Y} mutants alone (**Figure 7B**). This implies that the addition of the *R26R*$^{Fgfr2c;\beta act}$ allele increases sutural proliferation, which in turn delays osteogenic differentiation. This leads to bone hypoplasia and rescues the craniosynostosis phenotype.

Discussion

The paradox of FGFR2c signalling was first implicated when it was found that craniosynostosis can be caused by deletion of the IIIc isoform (*Fgfr2c*^{null}), as well as by introducing an activating mutation linked to human Crouzon syndrome (*Fgfr2c*^{C342Y}) (Eswarakumar et al., 2002, Eswarakumar et al., 2004). *Fgfr2c*^{C342Y} heterozygotes display an early postnatal craniosynostosis phenotype where *Fgfr2c*^{null} mice show late postnatal onset (Eswarakumar et al., 2004, Eswarakumar et al., 2002). We sought to increase our understanding of FGFR2c signalling misregulation through *Fgfr2c* overexpression and comparison to *Fgfr2c*^{C342Y}. Our data shows that global *Fgfr2c* overexpression yields craniofacial hypoplasia, microtia and cleft palate. Strikingly, this cohort of mutants did not develop coronal synostosis as opposed to *Fgfr2c*^{C342Y} and *Fgfr2c*^{null} mutants.

There are no reports of external ear defects related to human Crouzon syndrome or in *Fgfr2c*^{C342Y}mice. This study describes microtia with hypoplasia of the tympanic ring in *R26R*$^{Fgfr2c;\beta act}$ that has similarities to lacrimo-auriculo-dento-digital (LADD) syndrome which can be caused by mutations in *FGF10* or *FGFR2* (Rohmann et al., 2006). However, the external ear phenotype observed in the *R26R*$^{Fgfr2c;\beta act}$ is more likely to be a consequence of ectopic expression of FGFR2c in the ectoderm, potentially activated in an autocrine way by ectodermal FGF ligands with a high affinity for the IIIc isoform (Wright and Mansour, 2003). The lack of an external ear phenotype observed in other mouse models of *Fgfr2c* supports this (Eswarakumar et al., 2002, Eswarakumar et al., 2004). Nonetheless, a clear hypoplastic tympanic ring was noted in *R26R*$^{Fgfr2c;\beta act}$ mutants, a phenotype similar to *Fgfr2c*^{null} embryos at E18.5, implying the importance of FGFR2c in the osteogenesis of the auditory bulla (Eswarakumar et al., 2002).

Murine palatogenesis commence at E11.5 and is complete by E17.5 (Bush and Jiang, 2012). The prevalence of cleft palate in human Crouzon syndrome is less than that in Apert patients, which may be due to the mutation affecting both isoforms in the latter (Stanier and Pauws, 2012). The overt cleft phenotype in both *R26R*$^{Fgfr2c;\beta act}$ and *R26R*$^{Fgfr2c;Wnt1}$ was not fully penetrant: 40% (4/10) of *R26R*$^{Fgfr2c;\beta act}$ embryos and 16% (1/6) for *R26R*$^{Fgfr2c;Wnt1}$ respectively. As *Fgfr2b* is a major player for palatal shelf elevation, the partial penetrance implicates the IIIc isoform is less critical to this process, which is

supported by the observation that *Fgfr2c*^{null} mice do not have a cleft palate phenotype (Rice et al., 2004, Eswarakumar et al., 2002). However in the double mutants (i.e. *R26R*$^{Fgfr2c;\beta act}$; *Fgfr2c*^{C342Y}) the penetrance of cleft palate was 100% (n=7/7), indicating that the combination of the constitutively active receptor in with *Fgfr2c* overexpression exacerbates the cleft phenotype, resembling the *Fgfr2c*^{C342Y} homozygotes (Peskett et al., 2017).

Our data supports the conclusion that craniofacial hypoplasia is likely to be a result of conditional *Fgfr2c* overexpression in the neural crest (NC) lineage. A previous quantitative analysis of the adult *Fgfr2c*^{C342Y} reports smaller frontal and nasal bones, accompanied by a short anterior cranial base (Liu et al., 2013). Diminished calvarial bone volume was also reported in other mouse models for syndromic craniosynostosis most notably in *Fgfr2*^{S252W} and *Fgfr3*^{P244R} (Muenke syndrome) (Twigg et al., 2009, Chen et al., 2003). This is consistent with our finding that hypoplasia of NC derived bones is present in E18.5 *R26R*$^{Fgfr2c;\beta act}$ mice. Instead of a specific effect on NC derived tissues, it is also possible that ectopic expression of FGFR2c in the *R26R*$^{Fgfr2c;\beta act}$ mice plays a role. As mentioned before, expression of FGFR2 in the ectoderm is the likely explanation for the microtia phenotype. Similarly, ectopic expression in any other non-NC cells, or increased expression of FGFR2 in NC and mesoderm concomitantly during embryonic development of the head may contribute to the different craniofacial phenotype found in *R26R*$^{Fgfr2c;\beta act}$ mice compared to *R26R*$^{Fgfr2c;Wnt1}$ and *R26R*$^{Fgfr2c;Mesp1}$ mice. Interestingly, *Fgfr2c*^{C342Y} embryos at E18.5 do not show similar signs of hypoplasia at this stage. This is likely due to the nature of the C342Y mutation, which plays different roles in both early and late stages of development (Liu et al., 2013, Mansukhani et al., 2000). The C342Y mutation favours premature osteoblast commitment but inhibits bone mineralisation and facilitates cellular apoptosis during late gestation (Liu et al., 2013, Mansukhani et al., 2000, Rice et al., 1999). Despite similarities observed in the anterior bone phenotype of *Fgfr2c*^{C342Y} and *R26R*$^{Fgfr2c;\beta act}$, it is likely that the mechanism behind the phenotype is different. We propose that the hypoplasia found in *R26R*$^{Fgfr2c;\beta act}$ mutants is mainly a result of insufficient osteogenesis but we cannot exclude an ectopic effect at this stage.

A major difference between the *R26R*$^{Fgfr2c;\beta act}$ mice and *Fgfr2c*^{C342Y} mutants is the absence of coronal synostosis in the overexpression model. Neither do *R26R*$^{Fgfr2c;\beta act}$ mutants mimic the coronal synostosis phenotype of *Fgfr2c*^{null} mice. It is likely that the overall signalling disruption by receptor overexpression is less extreme than that of complete signalling removal (*Fgfr2c*^{null}) or a constitutively active receptor (*Fgfr2c*^{C342Y}). This is reflected by the relatively subtle phenotypic spectrum even with ubiquitous receptor overexpression under the control of the *βactin* promoter (*R26R*$^{Fgfr2c;\beta act}$). MAPK/ERK signalling is confined within a specific spatial domain along the membranous bones and the osteogenic fronts of the coronal suture. This was expected as the expression of *Spry* downstream targets coincides with periosteoblast cells known to be expressing *Fgfr2* (Deckelbaum et al., 2005, Johnson et al., 2000). Also, the relevant FGF ligands are confined to the osteogenic front. For example, *Fgf18* and *Fgf20* transcripts were detected in the osteogenic fronts of the coronal suture, coinciding with those genes involved in FGFR2 signalling, pointing towards potential autocrine interactions (Hajihosseini and Heath, 2002, Ornitz and Itoh, 2015). However, owing to the nature of ubiquitous overexpression and the morphogenic nature of FGFs, we expected ectopic expression to affect the *R26R*$^{Fgfr2c;\beta act}$ suture mesenchyme. The lack of phenotype in these overexpressing mutants suggests that while pERK is upregulated in both *Fgfr2c*^{C342Y} and *R26R*$^{Fgfr2c;\beta act}$, only *Fgfr2c*^{C342Y} sutures show increased differentiation as shown by increased levels of alkaline phosphatase, hence the craniosynostosis phenotype. Together this suggest that augmentation of MAPK/ERK signalling in the suture alone is not sufficient to derive a coronal synostosis phenotype in the craniofacial skeleton (Eswarakumar et al., 2004, Pfaff et al., 2016, Li et al., 2007).

Phenotypic rescue of the coronal suture could be generally achieved at the level of the receptor such as uncoupling Frs2 or through ERK knockdown (Eswarakumar et al., 2006, Shukla et al., 2007). Ultimately, the aim is to ameliorate Crouzon phenotype through FGFR2c signalling attenuation. We sought to address whether *Fgfr2c* overexpression is sufficient to delay ossification in *Fgfr2c*^{C342Y} given by the biochemical properties reported *in vitro* (Miraoui et al., 2009, Baddoo et al., 2003). Previous studies attempted to elucidate the paradoxical nature of FGFR2 signalling, where the perception of a GOF mutation leads towards signalling activity attenuation (Snyder-Warwick et al.,

2010, Pfaff et al., 2016, Bagheri-Fam et al., 2015). Specifically, two studies attempted to ameliorate phenotypes caused by the C342Y allele, by introducing the C342Y allele into the *Fgfr2c*^{null} background but yielded a more severe phenotypic spectrum (Pfaff et al., 2016, Bagheri-Fam et al., 2015). Our data suggests that the *Fgfr2c* overexpression allele was sufficient to delay synostosis. In particular, the extent of suture overlap in *R26R*$^{Fgfr2c;\beta act}$; *Fgfr2c*^{C342Y} mutants was decreased compared to control or *Fgfr2c*^{C342Y} mice. However, suture abolishment remains apparent due to the presence of the *Fgfr2c*^{C342Y} allele. As FGFR2 is critical for cell-renewal, one speculation for this rescue is shifting the balance from osteoblast differentiation to proliferation through 'scavenging activity' of endogenous FGF ligands by excess FGFR2c. Our results show that there is a distinct increase of proliferation in the sutural mesenchyme of *R26R*$^{Fgfr2c;\beta act}$; *Fgfr2c*^{C342Y} double mutants which would indicate a shift from differentiation to proliferation, explaining the osteogenic hypoplasia and the absence of craniosynostosis. This hypothesis is also supported by *in vitro* culture experiments with MSCs, as exposure to FGF2 promotes stemness in the presence of osteoblast differentiation media (Baddoo et al., 2003). Another possibility is that the addition of an extra wild-type *Fgfr2c* allele into the *Fgfr2c*^{C342Y} heterozygous mice disrupts the receptor turnover at the membrane and/or disturbs the dimerization equilibrium, favouring WT homodimers over WT/C342Y heterodimers. Altogether, the delayed synostosis in double mutants suggests *Fgfr2c* overexpression partially rescues reduced premature osteoblast commitment caused by the C342Y allele (Eswarakumar et al., 2004, Peskett et al., 2017).

We propose the FGFR2c paradox should not be based solely on the signalling amplitude but rather, the cascade FGFR2c transactivates. This is due to activation of TRK receptors, such as FGFR2, triggers signal transduction through three major cascades (PI3K-AKT, RAS-MAPK and PLCγ-PKC) (Ornitz and Itoh, 2015). It was previously reported that GOF mutations in the FGFR2c receptor elicit dissimilar cascade activation to that of WT-FGFR2c (Kim et al., 2003, Miraoui et al., 2009). Miraoui et al., 2009 compared the differences in cascade activation and concluded that Apert-FGFR2-S252W transactivates the PLCγ-PKC pathway to drive osteoblast differentiation and mineralisation, whereas WT-FGFR2 predominantly signals through the RAS-MAPK pathway (Miraoui et al., 2009). Other

growth factor pathways involving TRK receptors misregulation behave similarly, for example PDGFRα, where sustained activation of the receptor is responsible for complex craniosynostosis through PLCγ-PKC cascade (Moenning et al., 2009). Generally speaking, augmentation of RAS-MAPK signalling promotes proliferation whilst cellular differentiation is a consequence of cascade suppression (Dinsmore and Soriano, 2018). This cellular consequence is comparable to embryonic stem cells maintaining pluripotency (Yamanaka et al., 2010). For example, in the murine palate, it is understood that proliferation of palatal mesenchyme cells are driven by activated ERK through the exposure to FGFs in culture, and that its inhibition led to downregulation of 'stemness' genes (Vasudevan et al., 2015). In the same study, genetic ablation of *Fgfr1* (*Fgfr1*^{null}) led to ectopic osteoblast differentiation in the palatal shelves *in vivo* (Vasudevan et al., 2015). Unpublished data from this laboratory also supports this as oncogenic activation of KRas (i.e. KRas-G12D), an effector of the MAPK/ERK pathway in the NC lineage (*Kras*$^{G12D;Wnt1}$) led to severe craniofacial hypoplasia. Oncogenic KRas is known to cause terminal differentiation defects, suggesting upregulation of MAPK/ERK signalling alone resulted in insufficient osteoblast differentiation (Tuveson et al., 2004, Haston et al., 2017). Therefore, the pathogenic mechanism for craniosynostosis cannot be attributed to RAS/MAPK misregulation alone.

In summary, this study has demonstrated that FGFR2c overexpression yields craniofacial hypoplasia without a craniosynostosis phenotype. The most striking observation is the phenotypic variation between *R26R*$^{Fgfr2c;βact}$ and *Fgfr2c*^{C342Y} despite similarities in signalling dynamics. This implies that receptor overexpression and GOF mutations are mechanistically different, and require a different downstream interpretation to the WT. This is well characterised *in vitro* with preferential signal transduction, and our results relate these findings to an *in vivo* context. Maintaining the correct balance between proliferation and differentiation is crucial for osteogenesis and suture patency. Elucidating the role of FGFR2c signalling will improve the understanding of normal craniofacial development and its related pathologies, while providing a framework for the development of novel therapeutic strategies.

Materials and methods

Animals

Fgfr2c overexpression mouse (Gt(ROSA)26Sor$^{tm1(Fgfr2\text{-}IIIc)Pauw}$; aka *R26R*$^{Fgfr2c\text{-}flox}$; MGI:6150825). To target the *Rosa26* genomic locus (Gt(ROSA)26^{tm1Sor}), an *Fgfr2c* cDNA expression construct containing a V5 epitope on the C-terminal end of the protein was inserted into a targeting vector carrying the loxP-PGK-neo-tPa-loxP cassette (Soriano 1999), followed by homologous recombination and the creation of chimera. Germline mice carrying the *R26R*$^{Fgfr2c\text{-}flox}$ allele were backcrossed onto a CD1 background and maintained as homozygotes. To generate *Fgfr2c* overexpressing mutants, mice carrying the *R26R*$^{Fgfr2c\text{-}flox}$ allele were crossed with animals carrying a Cre recombinase allele (*βactin*^{CRE}; *Wnt1*^{CRE} or *Mesp1*^{CRE}). Embryos were genotyped for Cre recombinase and loxP excision. Genotyping primers are available upon request.

Crouzon mouse model (*Fgfr2*^{tm4Lni}; aka *Fgfr2c*^{C342Y}; MGI:3053095). *Fgfr2c*^{C342Y} were re-derived through the European Mouse Mutant Archive (EMMA) at MRC Harwell as previously described (Peskett et al., 2017).

Generation of double mutants was performed by crossing *R26R*$^{Fgfr2c\text{-}flox}$ animals with *Fgfr2c*^{C342Y} heterozygotes followed by genotyping for both alleles. *Fgfr2c*^{C342Y}; *R26R*$^{Fgfr2c\text{-}flox}$ animals were subsequently crossed with *βactin*^{CRE} to generate ubiquitous overexpression in the Crouzon mouse (i.e. *R26R*$^{Fgfr2c;\beta act}$;*Fgfr2c*^{C342Y}).

Wnt1^{CRE};*R26R*^{YFP} was as previously described (Freem et al., 2010). CRE recombinase is driven under the control of the *Wnt1* promoter to generate conditional expression in the NCC lineage. *Wnt1*^{CRE} mice were crossed with *R26R*$^{YFP/YFP}$ reporter to generate *Wnt1*$^{CRE/+}$; *R26R*$^{YFP/+}$ offspring. Cells positive with the *CRE* allele will express the reporter protein, thus labeling cells from the NCCs lineage.

R26R$^{mTmG/mTmG}$ were as previously described (Muzumdar et al., 2007). The *mTmG* allele was crossed with *R26R*$^{Fgfr2cV5/Fgfr2cV5}$ to generate a double conditional mouse that overexpresses both *mTmG* and *Fgfr2cV5* (*R26R*$^{mTmG/+}$; *R26R*$^{Fgfr2cV5/+}$) upon CRE deletion.

All animal procedures were performed in accordance with the UK Animals (Scientific Procedures) Act 1986 (Project License number: 70/8817) and maintained by UCL Biological Services.

Cells

Human embryonic kidney (HEK293T) cells were cultured in Minimum Essential Medium (MEM) alpha culture medium (Thermo Fisher Scientific) supplemented with 10% Fetal Bovine Serum (FBS) and Penicillin-Streptomycin. Cells were transfected with pcDNA3.1 (Invitrogen) plasmids containing a FGFR2c ORF (wild-type (WT) and C342Y) with a V5 tag on the C-terminal end, as well as control pcDNA3.1 without insert when they had reached 50% confluence. A cocktail of Optimem culture medium (Gibco), FuGENE transfection reagent (Promega) and plasmid DNA was added to each well prior to 48 hours incubation at 37°C, 5% CO2.

Immunoblots

E12.5 embryos were dissected under ice cold PBS and homogenized in RIPA buffer (150mM NaCl, 1% Triton X-100 (Fisher), 0.5% sodium deoxycholate (Sigma), 0.1% SDS (Sigma), 50mM Tris-pH 8.0 (Fisher)) with MINI complete protease inhibitor cocktail (Sigma) and centrifuged to obtain the lysates. Protein concentration was determined using Bradford reagent (Biorad) and spectrophotometry. A special cell lysis buffer (50mM pH7.6 Tris-Base; 150mM NaCl, 1% Triton X-100, 0.02% Sodium Azide, 1mM MINI protease inhibitor (Roche), 1mM sodium orthovanadate, 25mM sodium fluoride) was adopted for cells. Lysates were resolved, transferred and blotted using standard protocols. Anti-V5 antibody (Invitrogen) was used at a concentration of 1:1000 for E12.5 embryos and 1:3000 for cell lysates. Anti-pERK (1:2000, Cell Signalling Technology) and anti-tERK (1:2000, Cell Signalling Technology) were used to determine pathway activity. pERK blots were quantified by densitometry using FIJI software, and results expressed as the relative pERK:tERK ratio.

Quantitative RT-qPCR

RNA was extracted using the Trizol method (Invitrogen). Any genomic DNA was subsequently eliminated using the DNA-free DNA Removal Kit (Ambion) prior to RT reaction. QuantiTect Reverse Transcription Kit (Qiagen) was used for cDNA synthesis. cDNA was used for RT-qPCR reactions using Taqman assays (Applied Biosystems) according to the manufacturer's protocol. *Fgfr2c* assay (Applied Biosystems; Mm01269938_m1) was used to determine *Fgfr2c* overexpression. The collected dataset was analysed using the 7500 Fast Real-Time PCR System (Applied

Biosystems). Amplification efficiencies were checked for target genes and controls prior to data analysis using the ΔΔCt method.

***Ex vivo* calvarial explants**

A calvarial explant protocol was performed as previously described (Lana-Elola et al., 2007). Embryos were harvested at E17.5 and dissected in PBS. The calvaria was removed from the skin and brain and cultured in Dulbecco's Modified Eagle Medium (DMEM, Sigma) supplemented with 10% Fetal Bovine Serum (FBS, Sigma) and Penicillin-Streptomycin. The medium, with or without the addition of 10ng/ml FGF2, was refreshed every other day and cultured for 10-15 days at 37ºC, 5% CO_2. Calvaria were fixed in 90% ethanol and processed for Alizarin Red staining.

Gross phenotypic analysis

Embryos were weighed using a fine balance. An electronic caliper (Fisher) was used to measure the crown-rump length and head length of the embryo.

Wholemount skeletal staining

The procedure for wholemount skeleton histology was as previously described (Peskett et al., 2017). E18.5 embryos were skinned, eviscerated and fixed in 90% EtOH overnight at 4ºC and stained with Alcian Blue (Sigma) working reagent (0.01% Alcian Blue; 20% Acetic Acid; 80% of 75% EtOH) overnight at RT. Embryos were washed in 75% EtOH for a further 24 hours and cleared in 1% Potassium Hydroxide (KOH) the following day. After sufficient clearing, 0.01% Alizarin Red (Sigma) working solution (0.01% Alizarin Red in 1% KOH) was added to the embryos. The embryos were stained overnight and washed in 1% KOH the following day. Graded glycerol (Sigma) was used to prepare samples for imaging and long-term storage in 80% glycerol.

Quantitative analysis of the calvaria

Stained E18.5 calvaria were subjected to 'Region of Interest' (ROI) analysis using ImageJ 2.0 software (NIH). The craniofacial skeleton was dissected for the frontal, parietal and nasal bones in 80% glycerol and flat mounted onto frosted slides (Fisher). Images were taken for surface area measurements of frontal, parietal and nasal bones using ImageJ. Two measurements were made from both hemispheres of the bone, and the results were expressed as an average value. The quantification

was performed blind without knowledge of the embryo's genotype. The mandibles were quantified in the same manner with the length measured instead. Quantified data was normalised to limb length which provides an endogenous control that was unaffected by increased FGFR2c signalling (**Supplementary Figure 2**).

Statistical analysis

SPSS Statistics 22 (IBM) software was used as the primary statistical package for data analysis. First, the data was tested for normality using Shapiro-Wilk test to determine the use of parametric or non-parametric tests. Independent samples t-test with Welch's correction was used to compare the difference of means between the Control and mutant groups for quantification of gross phenotype and craniofacial skeleton. One-way ANOVA with Tukey posthoc or non-parametric Kruskal Wallis with Dunn-Bonferroni posthoc test was adopted for analysis of three or more groups. A p-value of <0.05 was considered significant. The analysed data were plotted using Prism 6.0 software (GraphPad).

Embryo embedding and histology

For paraffin embedding, E16.5 embryo heads were skinned and fixed in 10% Formalin overnight before graded dehydration in ethanol. Embryos were cleared in analytical grade xylene (Fisher) before paraffin wax displacement in a 60^{o}C oven. The samples were embedded and sectioned between 8-10um on the axial plane using a microtome (Leica). For frozen sections, E16.5 or E18.5 heads were embedded in OCT and snapped frozen using -80^{o}C isopentane method. Samples were sectioned between 15-20µm on the cryostat (Bright).

Immunofluorescence

Paraffin sections were dewaxed in Histoclear (National Diagnostics) before graded EtOH rehydration. Antigen retrieval was executed in a decloaking chamber (BioCare Medical) at 110^{o}C for 10 minutes in 10mM Sodium Citrate pH6.5 buffer. Sections were permeabilised in 0.1% PBST and blocked in 10% sheep serum (Sigma) and blocking Buffer (0.15% Glycine, 2mg/ml BSA in 0.1% PBST). Primary antibodies were incubated on the sections overnight in 1% sheep serum (Sigma) and blocking buffer. pERK (rabbit mIgG, Cell Signalling Technology) was used at 1:200, and appropriate secondary antibodies were incubated for an hour the following day. Biotin goat-anti-rabbit Alexa

Fluor 488 secondaries (Dako) were used against pERK. The pERK signals were amplified using Streptavidin 555 conjugates (Life Technologies) at 1:500. 0.1% Sudan black was applied onto tissue sections for 5 minutes to quench any autofluorescence, and rinsed briefly in PBST to relieve any excess staining. Lastly, tissue sections were stained in DAPI (Thermo Fisher) at 1:10,000 in PBS before coverslipped in Mowiol mounting medium (Sigma).

Phospho-Histone-H3 (pHH3) immunofluorescence

Standard immunofluorescence was performed on E18.5 cryosectioned heads. Briefly, cryosections were thawed at RT in a humidified chamber and rehydrated in PBS before fixation in 4% PFA, before 0.1% PBST permeabilisation and non-specific binding blocked in sheep serum as described above. Anti-pHH3 (rabbit polyclonal IgG, Millipore) was incubated overnight at a concentration of 1:100 in blocking buffer prior to Alexa Fluor 488 (Invitrogen) secondary antibody detection at a concentration of 1:250 against host specie. Further washes in 0.1% PBST was carried out prior to DAPI-PBS nuclei staining as described above. Sections were coverslipped in Mowiol mounting medium (Sigma) as described above. Quantitation of pHH3 cells was achieved using a macro written for FIJI software. Mitotic index is expressed as a percentage of the total pHH3 cells in respect to the total number of nuclei. The output is subsequently processed for statistical analysis using SPSS (IBM).

Alkaline phosphatase assay

Cryosectioned embryos were thawed and immediately fixed in 4% PFA before permeabilisation in 0.1% TBST. Samples were equilibrated in NTMT before developing in NBT-BCIP solution. Developed samples were counterstained with nuclear fast red (Sigma) and mounted in Mowiol mounting media (Sigma).

Competing interests

The authors have no competing or financial interests to declare.

Acknowledgements

We thank Albert Basson (King's College London) for the *Spry2, Spry4* and *Etv5* plasmids. *Fgfr2c*^{C342Y} mouse colony was derived from the EMMA Consortium. This work was supported by Great Ormond Street Hospital Children's Charity (award 09ND12) and University College London. K.K.L.L is a recipient of the UCL-GOSHCC IMPACT PhD studentship. P.S. is supported by a GOSHCC leadership award and E.Pa. is a GOSHCC Principal Investigator (award W0908). Microscopy was performed at the Light Microscopy Core Facility, UCL GOS Institute of Child Health supported by the NIHR GOSH BRC (award 17DD08). This research was supported by the NIHR Great Ormond Street Hospital Biomedical Research Centre. The views expressed are those of the author(s) and not necessarily those of the NHS, the NIHR or the Department of Health.

References

BADDOO, M., HILL, K., WILKINSON, R., GAUPP, D., HUGHES, C., KOPEN, G. C. & PHINNEY, D. G. 2003. Characterization of mesenchymal stem cells isolated from murine bone marrow by negative selection. *J Cell Biochem,* 89**,** 1235-49.

BAGHERI-FAM, S., ONO, M., LI, L., ZHAO, L., RYAN, J., LAI, R., KATSURA, Y., ROSSELLO, F. J., KOOPMAN, P., SCHERER, G., BARTSCH, O., ESWARAKUMAR, J. V. P. & HARLEY, V. R. 2015. FGFR2 mutation in 46,XY sex reversal with craniosynostosis. *Human Molecular Genetics,* 24**,** 6699-6710.

BUSH, J. O. & JIANG, R. 2012. Palatogenesis: morphogenetic and molecular mechanisms of secondary palate development. *Development,* 139**,** 231-43.

CHEN, L., LI, D., LI, C., ENGEL, A. & DENG, C. X. 2003. A Ser252Trp [corrected] substitution in mouse fibroblast growth factor receptor 2 (Fgfr2) results in craniosynostosis. *Bone,* 33**,** 169-78.

DECKELBAUM, R. A., MAJITHIA, A., BOOKER, T., HENDERSON, J. E. & LOOMIS, C. A. 2005. The homeoprotein engrailed 1 has pleiotropic functions in calvarial intramembranous bone formation and remodeling. *Development,* 133**,** 63.

DINSMORE, C. J. & SORIANO, P. 2018. MAPK and PI3K signaling: At the crossroads of neural crest development. *Dev Biol*.

ESWARAKUMAR, V. P., HOROWITZ, M. C., LOCKLIN, R., MORRISS-KAY, G. M. & LONAI, P. 2004. A gain-of-function mutation of Fgfr2c demonstrates the roles of this receptor variant in osteogenesis. *Proceedings of the National Academy of Sciences of the United States of America,* 101**,** 12555-12560.

ESWARAKUMAR, V. P., LAX, I. & SCHLESSINGER, J. 2005. Cellular signaling by fibroblast growth factor receptors. *Cytokine & Growth Factor Reviews,* 16**,** 139-149.

ESWARAKUMAR, V. P., MONSONEGO-ORNAN, E., PINES, M., ANTONOPOULOU, I., MORRISS-KAY, G. M. & LONAI, P. 2002. The IIIc alternative of Fgfr2 is a positive regulator of bone formation. *Development,* 129**,** 3783-3793.

ESWARAKUMAR, V. P., ÖZCAN, F., LEW, E. D., BAE, J. H., TOMÉ, F., BOOTH, C. J., ADAMS, D. J., LAX, I. & SCHLESSINGER, J. 2006. Attenuation of signaling pathways

stimulated by pathologically activated FGF-receptor 2 mutants prevents craniosynostosis. *Proceedings of the National Academy of Sciences,* 103**,** 18603-18608.

FREEM, L. J., ESCOT, S., TANNAHILL, D., DRUCKENBROD, N. R., THAPAR, N. & BURNS, A. J. 2010. The intrinsic innervation of the lung is derived from neural crest cells as shown by optical projection tomography in Wnt1-Cre;YFP reporter mice. *J Anat,* 217**,** 651-64.

HAJIHOSSEINI, M. K. & HEATH, J. K. 2002. Expression patterns of fibroblast growth factors-18 and -20 in mouse embryos is suggestive of novel roles in calvarial and limb development. *Mechanisms of Development,* 113**,** 79-83.

HASTON, S., POZZI, S., CARRENO, G., MANSHAEI, S., PANOUSOPOULOS, L., GONZALEZ-MELJEM, J. M., APPS, J. R., VIRASAMI, A., THAVARAJ, S., GUTTERIDGE, A., FORSHEW, T., MARAIS, R., BRANDNER, S., JACQUES, T. S., ANDONIADOU, C. L. & MARTINEZ-BARBERA, J. P. 2017. MAPK pathway control of stem cell proliferation and differentiation in the embryonic pituitary provides insights into the pathogenesis of papillary craniopharyngioma. *Development,* 144**,** 2141-2152.

ISEKI, S., WILKIE, A. O., HEATH, J. K., ISHIMARU, T., ETO, K. & MORRISS-KAY, G. M. 1997. Fgfr2 and osteopontin domains in the developing skull vault are mutually exclusive and can be altered by locally applied FGF2. *Development,* 124**,** 3375-3384.

JOHNSON, D., ISEKI, S., WILKIE, A. O. M. & MORRISS-KAY, G. M. 2000. Expression patterns of Twist and Fgfr1, -2 and -3 in the developing mouse coronal suture suggest a key role for Twist in suture initiation and biogenesis. *Mechanisms of Development,* 91**,** 341-345.

JOHNSON, D. & WILKIE, A. O. 2011. Craniosynostosis. *Eur J Hum Genet,* 19**,** 369-76.

KIM, H. J., KIM, J. H., BAE, S. C., CHOI, J. Y., KIM, H. J. & RYOO, H. M. 2003. The protein kinase C pathway plays a central role in the fibroblast growth factor-stimulated expression and transactivation activity of Runx2. *J Biol Chem,* 278**,** 319-26.

LANA-ELOLA, E., RICE, R., GRIGORIADIS, A. E. & RICE, D. P. 2007. Cell fate specification during calvarial bone and suture development. *Dev Biol,* 311**,** 335-46.

LEE, K., STANIER, P. & PAUWS, E. Mouse models of syndromic craniosynostosis. *Molecular Syndromology,* in press.

LI, C., SCOTT, D. A., HATCH, E., TIAN, X. & MANSOUR, S. L. 2007. Dusp6 (Mkp3) is a negative feedback regulator of FGF-stimulated ERK signaling during mouse development. *Development,* 134**,** 167-176.

LIU, J., NAM, H. K., WANG, E. & HATCH, N. E. 2013. Further analysis of the Crouzon mouse: effects of the FGFR2(C342Y) mutation are cranial bone-dependent. *Calcif Tissue Int,* 92**,** 451-66.

MANSUKHANI, A., BELLOSTA, P., SAHNI, M. & BASILICO, C. 2000. Signaling by Fibroblast Growth Factors (Fgf) and Fibroblast Growth Factor Receptor 2 (Fgfr2)–Activating Mutations Blocks Mineralization and Induces Apoptosis in Osteoblasts. *The Journal of Cell Biology,* 149**,** 1297-1308.

MIRAOUI, H., OUDINA, K., PETITE, H., TANIMOTO, Y., MORIYAMA, K. & MARIE, P. J. 2009. Fibroblast Growth Factor Receptor 2 Promotes Osteogenic Differentiation in Mesenchymal Cells via ERK1/2 and Protein Kinase C Signaling. *Journal of Biological Chemistry,* 284**,** 4897-4904.

MOENNING, A., JAGER, R., EGERT, A., KRESS, W., WARDELMANN, E. & SCHORLE, H. 2009. Sustained platelet-derived growth factor receptor alpha signaling in osteoblasts results in craniosynostosis by overactivating the phospholipase C-gamma pathway. *Mol Cell Biol,* 29**,** 881-91.

MUZUMDAR, M. D., TASIC, B., MIYAMICHI, K., LI, L. & LUO, L. 2007. A global double-fluorescent Cre reporter mouse. *Genesis,* 45**,** 593-605.

ORNITZ, D. M. & ITOH, N. 2015. The Fibroblast Growth Factor signaling pathway. *Wiley Interdisciplinary Reviews: Developmental Biology,* 4**,** 215-266.

ORR-URTREGER, A., BEDFORD, M. T., BURAKOVA, T., ARMAN, E., ZIMMER, Y., YAYON, A., GIVOL, D. & LONAI, P. 1993. Developmental Localization of the Splicing Alternatives of Fibroblast Growth Factor Receptor-2 (FGFR2). *Developmental Biology,* 158**,** 475-486.

PESKETT, E., KUMAR, S., BAIRD, W., JAISWAL, J., LI, M., PATEL, P., BRITTO, J. A. & PAUWS, E. 2017. Analysis of the Fgfr2C342Y mouse model shows condensation defects due to misregulation of Sox9 expression in prechondrocytic mesenchyme. *Biol Open,* 6**,** 223-231.

PFAFF, M. J., XUE, K., LI, L., HOROWITZ, M. C., STEINBACHER, D. M. & ESWARAKUMAR, J. V. P. 2016. FGFR2c-mediated ERK–MAPK activity regulates coronal suture development. *Developmental Biology,* 415**,** 242-250.

REARDON, W., WINTER RM FAU - RUTLAND, P., RUTLAND P FAU - PULLEYN, L. J., PULLEYN LJ FAU - JONES, B. M., JONES BM FAU - MALCOLM, S. & MALCOLM, S. 1994. Mutations in the fibroblast growth factor receptor 2 gene cause Crouzon syndrome. *Nat Genet.,* 8**,** 98-103.

RICE, D. P., KIM, H. J. & THESLEFF, I. 1999. Apoptosis in murine calvarial bone and suture development. *Eur J Oral Sci,* 107**,** 265-75.

RICE, R., SPENCER-DENE, B., CONNOR, E. C., GRITLI-LINDE, A., MCMAHON, A. P., DICKSON, C., THESLEFF, I. & RICE, D. P. 2004. Disruption of Fgf10/Fgfr2b-coordinated epithelial-mesenchymal interactions causes cleft palate. *J Clin Invest,* 113**,** 1692-700.

ROHMANN, E., BRUNNER, H. G., KAYSERILI, H., UYGUNER, O., NURNBERG, G., LEW, E. D., DOBBIE, A., ESWARAKUMAR, V. P., UZUMCU, A., ULUBIL-EMEROGLU, M., LEROY, J. G., LI, Y., BECKER, C., LEHNERDT, K., CREMERS, C. W., YUKSEL-APAK, M., NURNBERG, P., KUBISCH, C., SCHLESSINGER, J., VAN BOKHOVEN, H. & WOLLNIK, B. 2006. Mutations in different components of FGF signaling in LADD syndrome. *Nat Genet,* 38**,** 414-7.

SHUKLA, V., COUMOUL, X., WANG, R.-H., KIM, H.-S. & DENG, C.-X. 2007. RNA interference and inhibition of MEK-ERK signaling prevent abnormal skeletal phenotypes in a mouse model of craniosynostosis. *Nat Genet,* 39**,** 1145-1150.

SNYDER-WARWICK, A. K., PERLYN, C. A., PAN, J., YU, K., ZHANG, L. & ORNITZ, D. M. 2010. Analysis of a gain-of-function FGFR2 Crouzon mutation provides evidence of loss of function activity in the etiology of cleft palate. *Proceedings of the National Academy of Sciences,* 107**,** 2515-2520.

STANIER, P. & PAUWS, E. 2012. Development of the lip and palate: FGF signalling. *Front Oral Biol,* 16**,** 71-80.

TUVESON, D. A., SHAW, A. T., WILLIS, N. A., SILVER, D. P., JACKSON, E. L., CHANG, S., MERCER, K. L., GROCHOW, R., HOCK, H., CROWLEY, D., HINGORANI, S. R., ZAKS,

T., KING, C., JACOBETZ, M. A., WANG, L., BRONSON, R. T., ORKIN, S. H., DEPINHO, R. A. & JACKS, T. 2004. Endogenous oncogenic K-rasG12D stimulates proliferation and widespread neoplastic and developmental defects. *Cancer Cell,* 5**,** 375-387.

TWIGG, S. R., HEALY, C., BABBS, C., SHARPE, J. A., WOOD, W. G., SHARPE, P. T., MORRISS-KAY, G. M. & WILKIE, A. O. 2009. Skeletal analysis of the Fgfr3(P244R) mouse, a genetic model for the Muenke craniosynostosis syndrome. *Dev Dyn,* 238**,** 331-42.

VASUDEVAN, H. N., MAZOT, P., HE, F. & SORIANO, P. 2015. Receptor tyrosine kinases modulate distinct transcriptional programs by differential usage of intracellular pathways. *Elife,* 4.

WILKIE, A. O. M. 1997. Craniosynostosis: Genes and Mechanisms. *Human Molecular Genetics,* 6**,** 1647-1656.

WRIGHT, T. J. & MANSOUR, S. L. 2003. FGF signaling in ear development and innervation. *Curr Top Dev Biol,* 57**,** 225-59.

YAMANAKA, Y., LANNER, F. & ROSSANT, J. 2010. FGF signal-dependent segregation of primitive endoderm and epiblast in the mouse blastocyst. *Development,* 137**,** 715-24.

YOSHIDA, T., VIVATBUTSIRI, P., MORRISS-KAY, G., SAGA, Y. & ISEKI, S. 2008. Cell lineage in mammalian craniofacial mesenchyme. *Mechanisms of Development,* 125**,** 797-808.

Figures

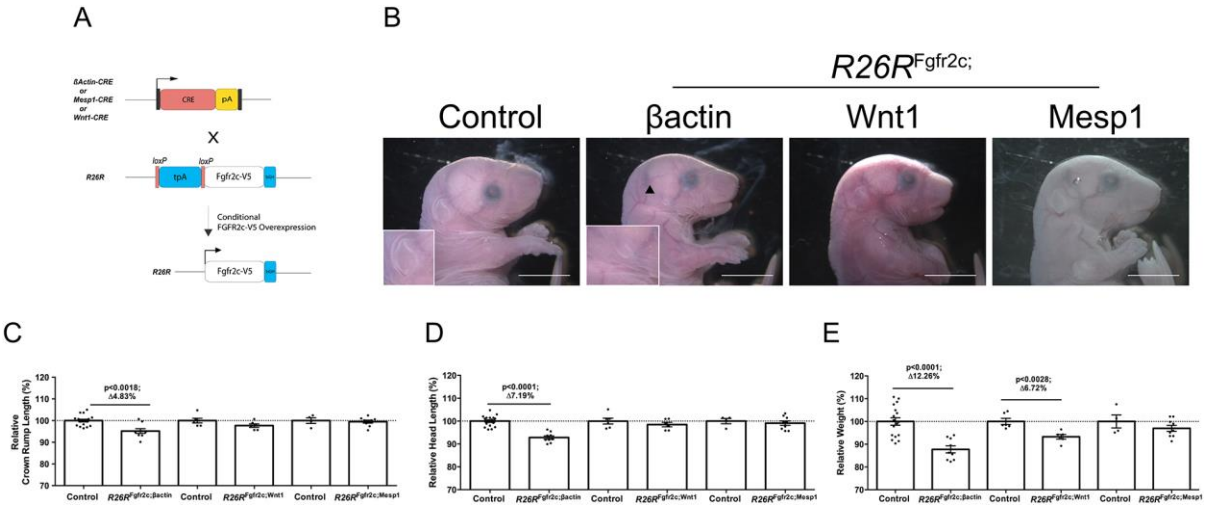

Figure 1 Gross phenotype of *Fgfr2c* overexpression in E18.5 mutants.

(**A**) Breeding strategy for conditional *Fgfr2c* overexpression. (**B**) Microtia (arrowhead + inset) in *R26R*$^{Fgfr2c;βact}$ only. (**C**) Skeletal hypoplasia in *R26R*$^{Fgfr2c;βact}$ ($p<0.0018$) (**D**) Craniofacial hypoplasia in *R26R*$^{Fgfr2c;βact}$ ($p<0.0001$) (**E**) *R26R*$^{Fgfr2c;βact}$ and *R26R*$^{Fgfr2c;Wnt1}$ display significant reductions in weight ($p<0.0001$ and $P<0.0028$ respectively). Statistics: Students t-test with Welch's correction. Scale bar: 5mm.

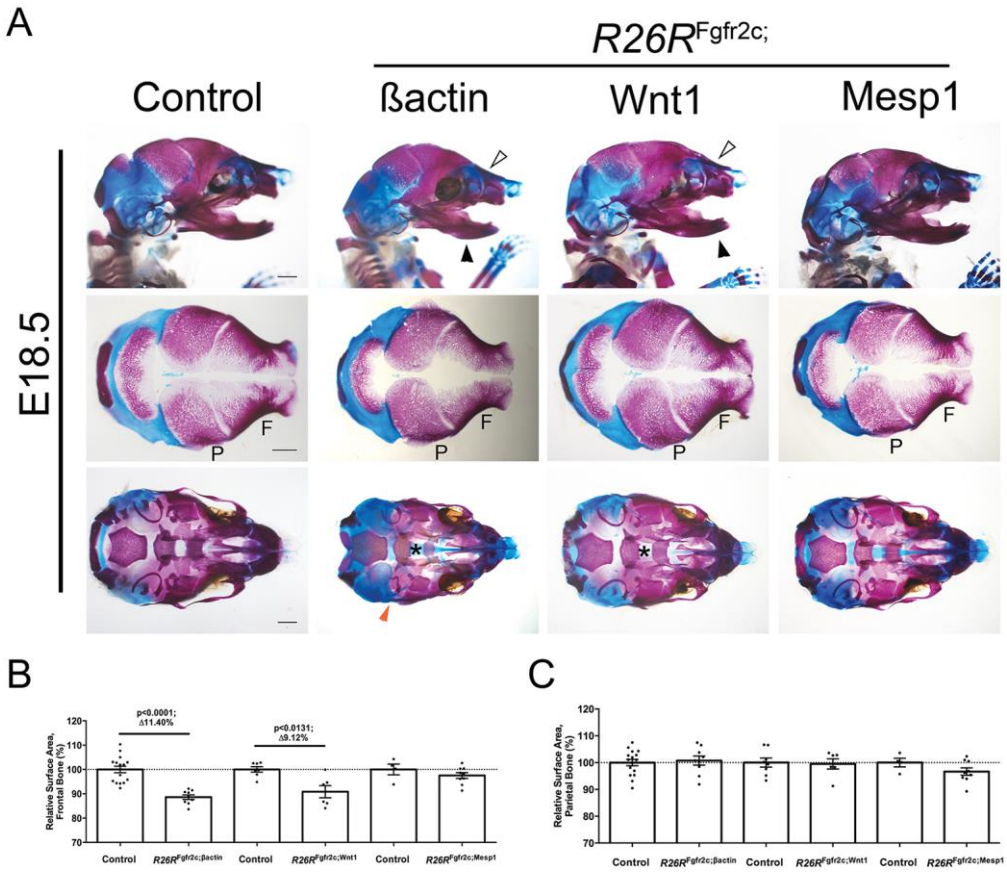

Figure 2 Craniofacial hypoplasia of the NCC lineage in E18.5 mutants.

(**A**) *R26R*$^{Fgfr2c;\beta act}$ and *R26R*$^{Fgfr2c;Wnt1}$ embryos display reductions of the nasal bones and mandibles (white and black arrowheads respectively). Other features include an overt cleft palate (asterisk) in *R26R*$^{Fgfr2c;\beta act}$, but only partially penetrant in *R26R*$^{Fgfr2c;Wnt1}$ embryos. Tympanic ring hypoplasia is exclusive to *R26R*$^{Fgfr2c;\beta act}$ embryos (red arrowhead). No apparent phenotype was observed in *R26R*$^{Fgfr2c;Mesp1}$ mice. (**B**, **C**) Quantitative analysis of the frontal and parietal bones. Significant reductions of the frontal bone in both *R26R*$^{Fgfr2c;\beta act}$ ($p<0.0001$) and *R26R*$^{Fgfr2c;Wnt1}$ embryos ($p<0.0131$). Statstics: Student's t-test with Welch's correction. Scale bar: 1mm.

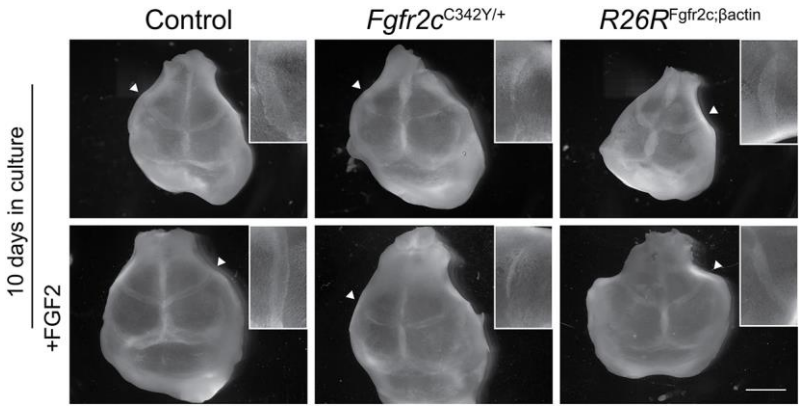

Figure 3 Calvarial explant culture of *Fgfr2c*^{C342Y} and *R26R*$^{Fgfr2c;\beta act}$ mutants.

Whole calvaria after 10 days in culture show partial fusion in *Fgfr2c*^{C342Y} heterozygous skulls (arrowhead, insert), while in *R26R*$^{Fgfr2c;\beta act}$ calvaria the coronal suture appears patent, resembling the control. Calvaria cultured with the addition of FGF2 ligand are undistinguishable from those without FGF2. Inserts are a magnified image of the representative coronal suture in the respective explants. Scale bar: 1mm.

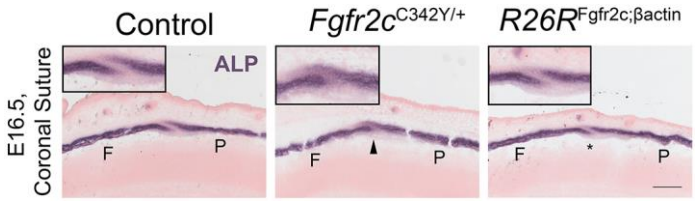

Figure 4 Alkaline phosphatase (ALP) activity in the coronal suture.

Fgfr2c^{C342Y} and *R26R*$^{Fgfr2c;\beta act}$ have dissimilar osteoblast activity in the E16.5 coronal suture. Increased appositional growth of *Fgfr2c*^{C342Y} sutures (arrow) and ectopic expression of ALP in sutural mesenchyme precedes synostosis while *R26R*$^{Fgfr2c;\beta act}$ sutures (*) resemble controls. Insert is a magnified crop of the suture. F: Frontal bone, P: Parietal bone; Scale bar: 200μm.

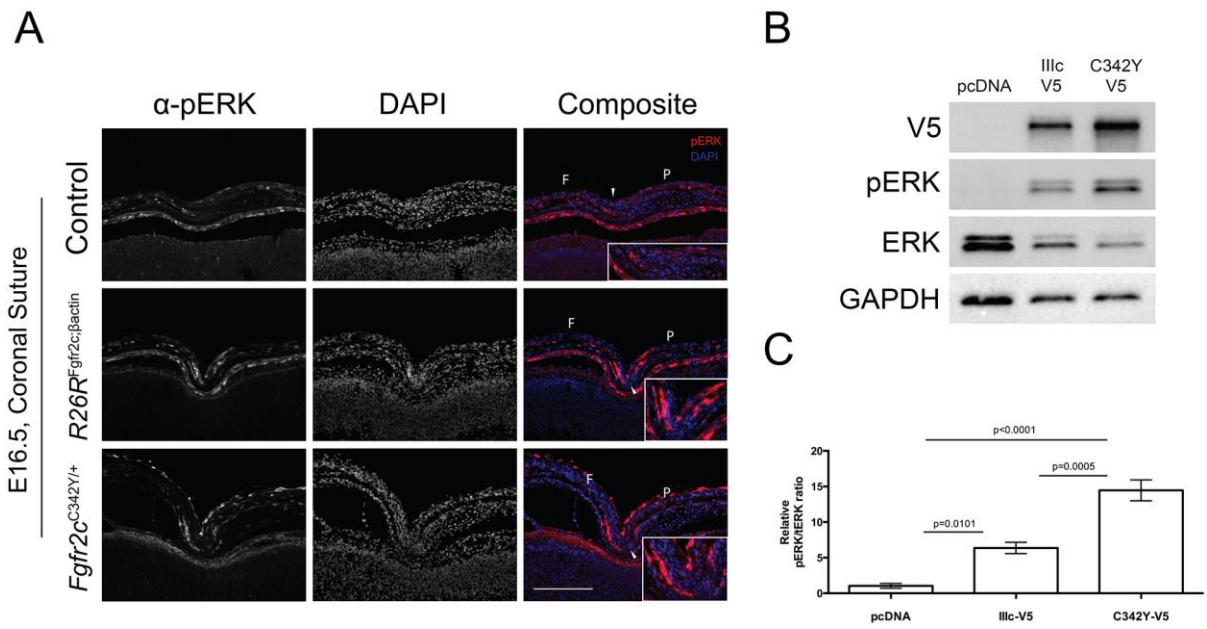

Figure 5 *Fgfr2c* overexpression causes upregulation of pERK *in vivo* and *in vitro.*

(**A**) Both *Fgfr2c*^{C342Y} and *R26R*$^{Fgfr2c;βact}$ mutants have upregulated pERK (red) in osteogenic fronts of frontal and parietal bones as compared to controls *in vivo*. (**B**) Western blot to demonstrate upregulation of pERK upon cellular transfection of pFGFR2c(WT)V5 (encoding the wild-type FGFR2-IIIc isoform) and pFGFR2c(C342Y)V5 (encoding the mutated receptor) plasmids in HEK293T cells. (**C**) Relative pERK:tERK ratio quantified by densitometry of transfected HEK293T cells. F: Frontal bone; P: Parietal bone; White arrowhead marks the location of the coronal suture. Insert is a cropped image of the coronal suture. Statistics: Oneway ANOVA with Tukey posthoc. Error bars: SEM. Scale Bar: 200μm.

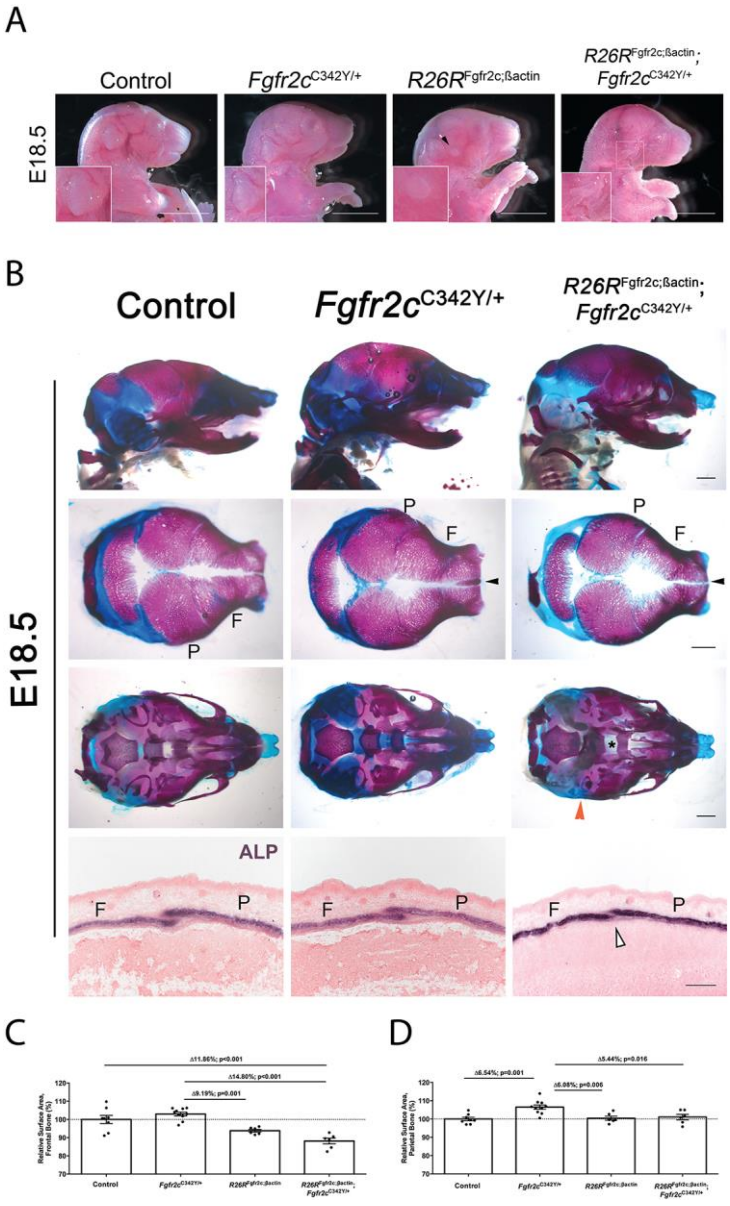

Figure 6 Phenotypic analysis of *R26R*$^{Fgfr2c;\beta act}$; *Fgfr2c*^{C342Y} double mutants at E18.5.

(**A**) *R26R*$^{Fgfr2c;\beta act}$; *Fgfr2c*^{C342Y} have a more severe phenotype of the external ear (box) compared to *R26R*$^{Fgfr2c;\beta act}$ (arrow). Inserts are magnified representations of the ear phenotype. (**B**) Craniofacial phenotype of the *R26R*$^{Fgfr2c;\beta act}$; *Fgfr2c*^{C342Y}. Wormian bone rescue in *R26R*$^{Fgfr2c;\beta act}$; *Fgfr2c*^{C342Y} and a wider frontal posterior interfrontal suture. Other features include severe tympanic ring hypoplasia and cleft palate. Bottom panels are ALP assays, notice partial sparing of the coronal suture in *R26R*$^{Fgfr2c;\beta act}$; *Fgfr2c*^{C342Y}. (**C**, **D**) Quantitative analysis of the calvarial bones. Significant size reduction of the frontal and parietal bones in *R26R*$^{Fgfr2c;\beta act}$; *Fgfr2c*^{C342Y} compared to *Fgfr2c*^{C342Y}

($p<0.001$ and $p=0.016$ respectively). Statistics: One way ANOVA with Tukey's Posthoc ; Arrows indicate regions affected. Scale bar: 1mm.

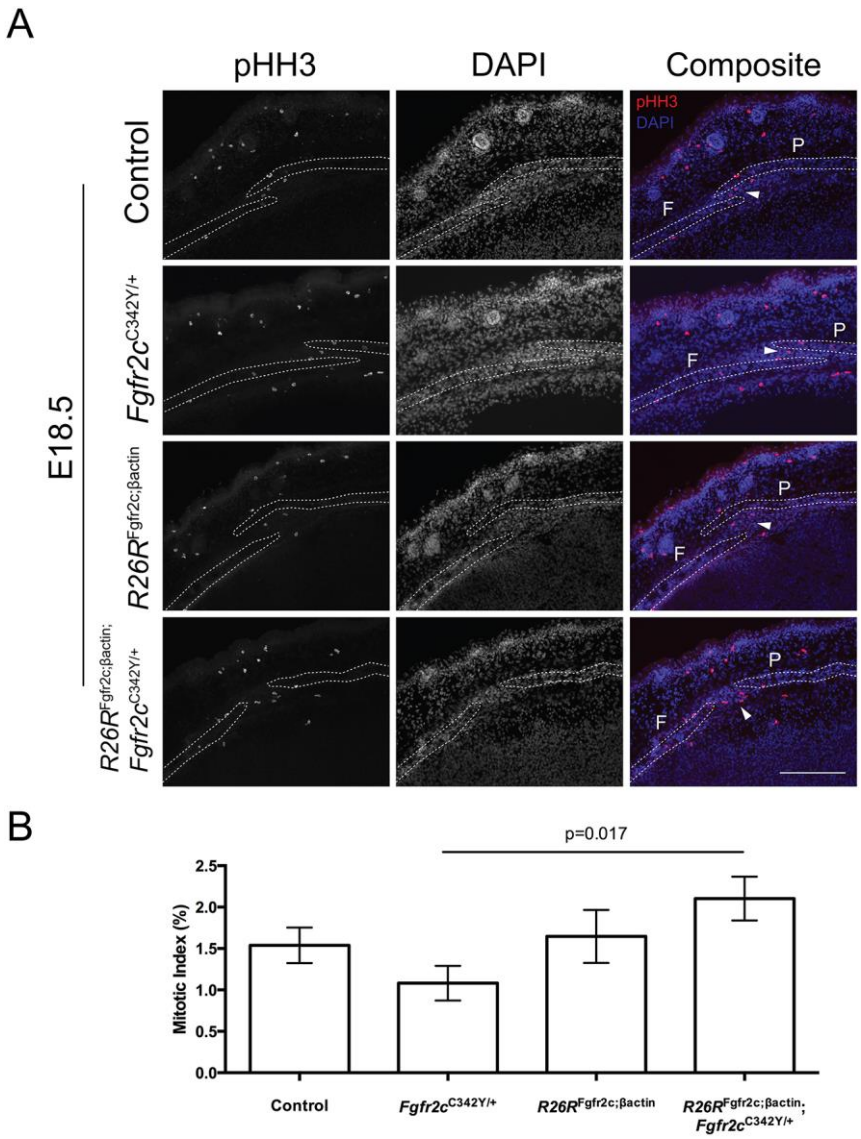

Figure 7 Analysis of proliferation by phoshohistone-3 immunohistochemistry.

(**A**) PHH3 staining (red) in sagittal sections through the coronal suture of *R26R*$^{Fgfr2c;\beta act}$ and *Fgfr2c*^{C342Y} single mutants, and *R26R*$^{Fgfr2c;\beta act}$; *Fgfr2c*^{C342Y} double mutants shows an apparent increased number of proliferative cells in the suture mesenchyme (white arrowheads) of double mutants. (**B**) Quantification of the proliferation assay shows a statistically significant increase ($P<0.05$) in *R26R*$^{Fgfr2c;\beta act}$; *Fgfr2c*^{C342Y} double mutants alone compared to *Fgfr2c*^{C342Y}. Scale bar is 200μm.

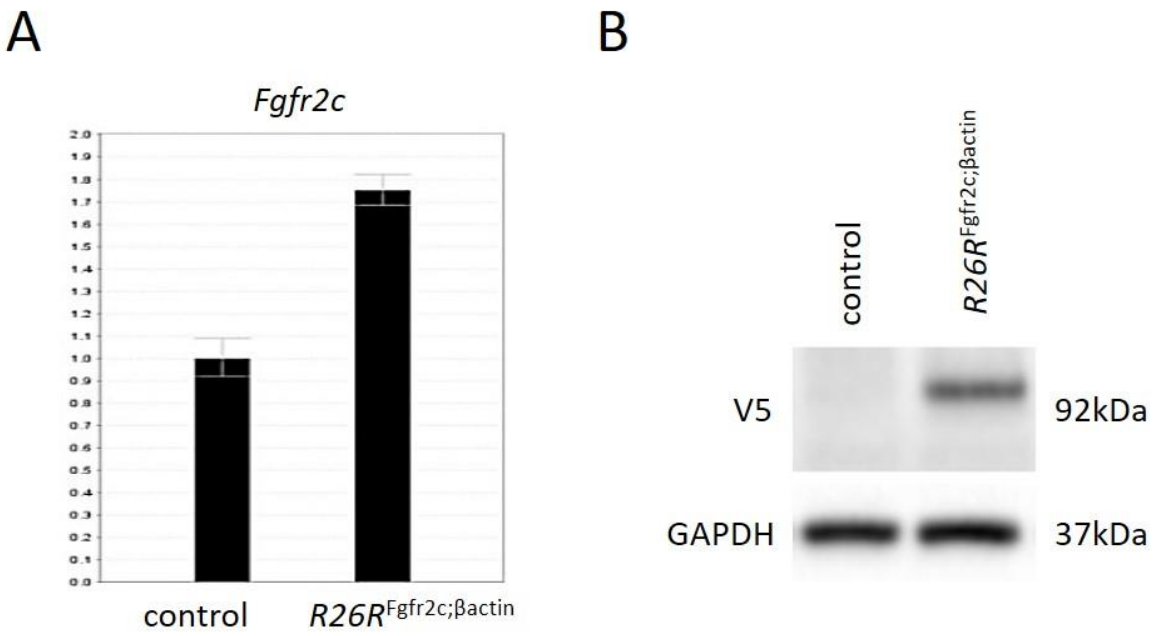

Figure S1. *Fgfr2c* RNA and FGFR2c protein expression validation.

(**A**) RT-qPCR analysis of *Fgfr2c* expression reveals upregulation of *Fgfr2c* transcripts by approximately 2-fold in *R26R*$^{Fgfr2c;\beta actin}$ E12.5 embryos. (**B**) Immunoblot for the V5 epitope shows expression of the transgenic FGFR2cV5 protein in overexpression embryos only.

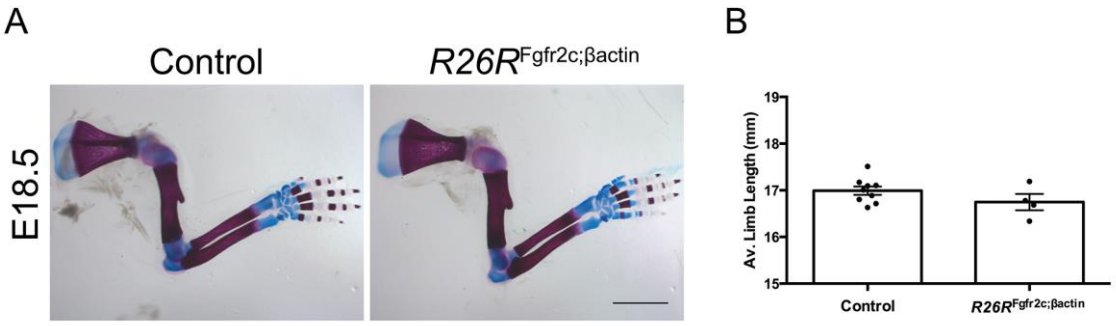

Figure S2. Quantitative analysis of *R26R*$^{Fgfr2c;\beta act}$ limb bones.

(**A**) Whole mount skeletal stained limbs of control and *R26R*$^{Fgfr2c;\beta act}$ E18.5 embryos show normal morphology.

(**B**) Quantitative analysis shows no statistically significant difference between control and mutant limb size.

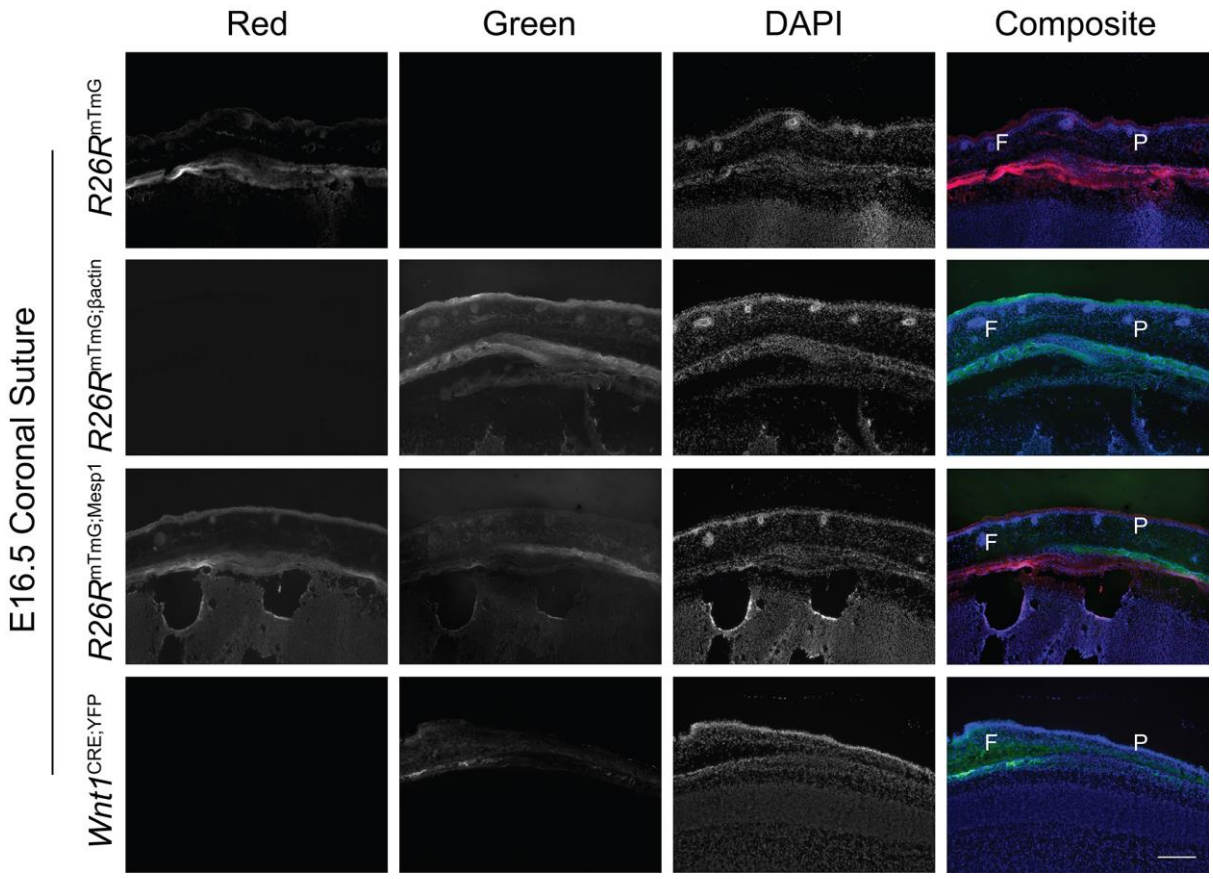

Figure S3. Reporter activity of *βactinCRE/+*, *Mesp1CRE/+* and *Wnt1CRE/+*.

eGFP (green) is only expressed in the event of CRE recombination in *R26RmTmG*, tdTomato (red) is expressed otherwise. Complete recombination is present in *R26RmTmG/+; βactinCRE/+*. Cells derived from the mesoderm are only present in the parietal bone of *R26RmTmG/+;Mesp1CRE/+*. Cells derived from the NCC lineage are only present in the frontal bone of *Wnt1CRE/+;YFP* mice. F:frontal bone, P: parietal bone; Scale bar: 200µm.

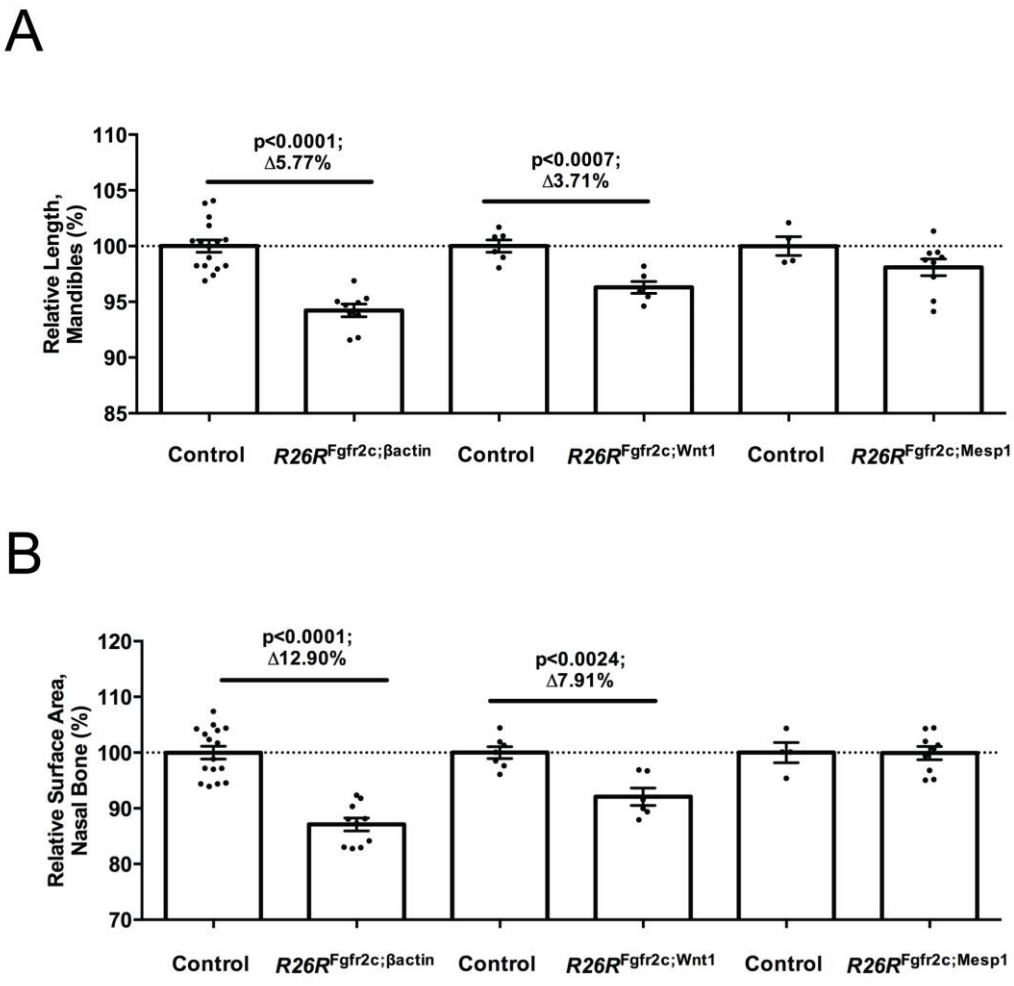

Figure S4. Quantitative analysis of neural crest derivatives in the craniofacial skeleton shows a decrease in size of mandible (**A**) and nasal bones (**B**) in *R26R*$^{Fgfr2c;\beta act}$ and *R26R*$^{Fgfr2c;Wnt1}$ E18.5 embryos. Statistics: Student's t-test with Welch's correction.